

The effect of time steps and time-scales on parametrization suites

David L. Williamson*

National Center for Atmospheric Research,[†] Boulder, CO, USA

*Correspondence to: David L. Williamson, PO Box 3000, NCAR, Boulder, CO 80307-3000, USA.
E-mail: wmson@ucar.edu

[†]The National Center for Atmospheric Research is sponsored by the National Science Foundation.

The problem of intense, truncation-scale storms that form in high-resolution versions of the Community Atmosphere Model Version 4 (CAM4) is studied. These storms are characterized by extreme vertical motion and heavy precipitation. This problem arises when some individual parametrizations do not produce an atmospheric-like state because they are restrained by the time-scales assumed in their formulation; other unconstrained parametrizations that follow then work in unintended ways. The behaviour of the moist parametrization components is examined in CAM4 for one typical, strong cell. At $T340$ spectral truncation with a 5 min time step, the deep and shallow convection parametrizations do not remove instabilities and supersaturation because they have time-scales of 1 h and 30 min, respectively. Then the prognostic cloud-water scheme, which is not constrained by a time-scale, does remove supersaturation. That local release of latent heat drives very strong vertical motion and horizontal convergence, which transports even more water vapour into the column, exacerbating the problem. Two simple model problems are introduced that illustrate the ramifications of the time-scale and time-step mismatch. When either the time-scales are shortened or the time step is lengthened, the convection parametrizations are more active and strong storms do not form. Copyright © 2012 Royal Meteorological Society

Key Words: Community Atmosphere Model; convective parametrization; moist parametrization; time splitting; process splitting; grid-point storms

Received 19 August 2011; Revised 16 April 2012; Accepted 15 May 2012; Published online in Wiley Online Library 8 August 2012

Citation: Williamson DL. 2013. The effect of time steps and time-scales on parametrization suites. *Q. J. R. Meteorol. Soc.* **139**: 548–560. DOI:10.1002/qj.1992

1. Introduction

Time-split and process-split approximations are common in Atmospheric General Circulation Models (AGCMs). Split forms are a convenient way to isolate the solution of each component of a model. In doing so they allow some degree of linearization and implicitness in approximations for each process without requiring the solution of a complex coupled system of equations. Williamson (2002) describes the choices made for the splitting approximations adopted in the Community Climate Model Version 3 (CCM3; Kiehl *et al.*, 1996, 1998) and for the modifications that were adopted in the subsequent Community Atmosphere Models, CAM2

(Collins *et al.*, 2003), CAM3 (Collins *et al.*, 2004, 2006) and CAM4 (Neale *et al.*, 2011), which evolved from CCM3. These include both the choices for the components within the parametrization suite and the choices for coupling the suite with different dynamical cores. He also reviews the studies of different coupling methods that had been applied in various atmospheric models up to that time. Williamson (2007) describes more recent studies on the coupling between the dynamical core and the parametrization suite.

Recently, a problem was noticed in a high-resolution version of CAM4 that arises with the time-split approximations in the parametrization suite, but, as will be argued

later, is actually associated with assuming different time-scales in different, potentially competitive parametrizations. The problem is excessive precipitation at spatial scales near the truncation limit, i.e. over three to four grid intervals. We will argue later that the problem would also occur if the parametrization components adopted process splitting within the suite.

We review some aspects of time-split approximations to introduce concepts that will be relevant when considering time-scales. Time-split approximations can be thought of as a sequential application or solution of each individual process. The initial state for each process is the solution from the preceding process in the splitting sequence. The goal in atmospheric modelling is for the temporal evolution of the model to match that of the atmosphere. We refer to that model evolution as the solution trajectory, i.e. the evolution or path in time of state variables that define the solution. (This is distinct from trajectories in physical space, which are calculated from the wind field.) In a forecast application the model trajectory should follow the corresponding atmospheric trajectory as closely as possible. In climate simulations the model trajectory should follow an atmospheric-like trajectory, a corresponding atmospheric trajectory not being known because of the lack of deterministic predictability after a few weeks of simulation. At the end of each time step, after all the processes in a time step have been completed, the solution should be as near as possible to an atmosphere-like trajectory, i.e. the model state should resemble an atmospheric state. This state represents model grid scales consistent with the numerical approximations and truncation, not point-wise atmospheric values. During the time-split sequence, individual processes may take the solution away from the atmospheric trajectory while others may return it toward the atmospheric trajectory. For example, moisture convergence by the dynamics may lead to supersaturation, a non-atmospheric-like state, and a parametrization may subsequently remove the supersaturation via condensation, returning the state to an atmospheric-like one. One implication of time splitting is that some of the split processes might have to work from non-atmospheric-like states, since previous processes might move the solution off an atmospheric trajectory or not completely return it to one. Currently they may or may not be deliberately designed to take this into account. Supersaturation is an example of such a non-atmospheric-like state.

For fluid-flow problems without a parametrization component, Strang (1968) proposed a spatial dimensional splitting sequence that divided the calculation into a sequence of one-dimensional calculations in each spatial dimension. He devised a formally higher-order accurate scheme by reversing the splitting order each time step, i.e. for two-dimensional advection his approach would calculate advection in the x direction first followed by advection in the y direction, then again in the y direction followed by that in the x direction. These two processes, advection in the x and y directions, have similar time-scales. Sportisse (2000) showed that the classical error analysis of Strang can fail when the time step is larger than the fastest time-scale. This occurs when combining stiff and non-stiff operators. In such a situation, the order of the splitting is crucial for accuracy and the stiff operator should be at the end of the splitting sequence because it tends to bring the state back to the desired trajectory. In our example above, the condensation

brings the solution closer to the atmosphere trajectory after the dynamics moved it away. Atmospheric modellers have intuitively applied the fast convection and condensation processes last, from the earliest days of numerical weather forecasting, to prevent the relative humidity from exceeding 100%. Williamson (2002) discusses these concepts in more detail. We do not provide a further discussion of splitting here since the main thrust of this article is related more to components with different time-scales coupled by splitting, but the concept of following an atmospheric-like trajectory as closely as possible is relevant.

As we will show in the following, the problem that arose in a high-resolution version of CAM4 alluded to earlier is associated with assuming a time-scale for one moist parametrization component that might be considered fast but makes it much slower than the time step and a second time-scale for another component that is comparable to the time step. In this situation the so-called fast component does not perform its action in a single time step and thus does not return the solution to an atmosphere trajectory consistent with the model spatial resolution. It would require multiple applications to do so, presumably over several time steps. However the second component completes the unfinished job even though it might not be intended to do so. If a non-atmospheric-like state sets up during the time-split sequence of a single time step, it seems reasonable that the parametrizations as a group should return the solution as close as possible to an atmospheric-like state, again consistent with the model resolution, but with each parametrization acting consistently with whatever it is parametrizing. Non-atmospheric-like conditions should be removed by the appropriate parametrization before the end of that time step in order for the solution trajectory to follow an atmospheric-like trajectory. This is not the case when parametrizations assume a relatively long time-scale compared to the time step, especially if only some do.

In the following we consider the consequences of a parametrization component not completing its process in a single application. We first consider two simple models. The first illustrates the consequences of having a single parametrization with a time-scale that is much longer than the time step in a time-split sequence. The second illustrates the consequence of having two parametrization components with very different time-scales. We then analyze the high-resolution CAM4 simulation that originally raised this issue and relate it to simple models. Finally we show that reducing the inconsistencies between the time step and time-scale ameliorates the problem.

2. Simple models

Consider a simple model that predicts specific humidity q with two processes, which we will refer to as dynamics (D) and parametrization (P). The prediction equation is

$$\frac{dq}{dt} = D + P. \quad (1)$$

The continuous problem we have in mind is one in which the dynamics transports water vapour into the grid box ($D > 0$) and once the box is saturated ($q = q_s$) the parametrization condenses the excess water vapour as fast as the dynamics creates supersaturation. Thus, once the grid box is saturated, $P = -D$, $dq/dt = 0$ and $q = q_s$.

We now consider a time-split approximation to (1) and an approximation to P. Assume the dynamics D alone provides a linear increase of q in time t at a constant rate α :

$$\frac{dq}{dt} = \alpha, \quad (2)$$

i.e. convergence of moisture into a region. The analytic solution of the dynamics D over a time interval Δt is

$$q^{t+\Delta t} = q^t + \alpha \Delta t, \quad (3)$$

where q^t is the solution at time t . Assume the parametrization P removes supersaturation. If q is supersaturated, the parametrization reduces q toward saturation q_s with a time-scale τ , otherwise it does nothing:

$$\frac{d(q - q_s)}{dt} = \begin{cases} -(q - q_s)/\tau & \text{if } q > q_s, \\ 0 & \text{if } q \leq q_s. \end{cases} \quad (4)$$

Such time-scales are included in both deep and shallow convection parametrization formulations in CAM4. Note that (4) is an approximation to the continuous P described following (1), but we can consider (2) as the correct D in (1). If q at time t is at least saturated, the analytic solution of the parametrization P over a time interval Δt is

$$(q^{t+\Delta t} - q_s) = (q^t - q_s) e^{-\Delta t/\tau}. \quad (5)$$

As described following (1), the conceptual 'atmospheric' trajectory in this simple problem is a saturated state with condensation balancing the moisture source.

Consider a time-split approximation to (1). Each split process is solved analytically (see (3) and (5)), and thus has no computational time-step restriction for stability. Let $t = n\Delta t$. The first split substep provides an intermediate forecast from the dynamics alone:

$$q^* = q^{n\Delta t} + \alpha \Delta t. \quad (6)$$

The second split substep calculates the parametrization based on that intermediate value:

$$(q^{(n+1)\Delta t} - q_s) = (q^* - q_s) e^{-\Delta t/\tau}. \quad (7)$$

Here we assume that q^* is at least saturated. Substituting (6) into (7) gives the forecast over one time step,

$$(q^{(n+1)\Delta t} - q_s) = [(q^{n\Delta t} - q_s) + \alpha \Delta t] e^{-\Delta t/\tau}. \quad (8)$$

Now consider a sequence of time steps. A first time step with $n = 0$ gives

$$(q^{\Delta t} - q_s) = [(q^0 - q_s) + \alpha \Delta t] e^{-\Delta t/\tau}. \quad (9)$$

A second step ($n = 1$) gives

$$(q^{2\Delta t} - q_s) = [(q^{\Delta t} - q_s) + \alpha \Delta t] e^{-\Delta t/\tau}. \quad (10)$$

Substitution of (9) into (10) gives

$$(q^{2\Delta t} - q_s) = (q^0 - q_s) e^{-2\Delta t/\tau} + \alpha \Delta t (e^{-2\Delta t/\tau} + e^{-\Delta t/\tau}). \quad (11)$$

A third step ($n = 2$) gives

$$(q^{3\Delta t} - q_s) = [(q^{2\Delta t} - q_s) + \alpha \Delta t] e^{-\Delta t/\tau}. \quad (12)$$

Substituting (11) into (12) gives

$$(q^{3\Delta t} - q_s) = (q^0 - q_s) e^{-3\Delta t/\tau} + \alpha \Delta t (e^{-3\Delta t/\tau} + e^{-2\Delta t/\tau} + e^{-\Delta t/\tau}). \quad (13)$$

One can now see that the general expression is

$$(q^{n\Delta t} - q_s) = (q^0 - q_s) e^{-n\Delta t/\tau} + \alpha \Delta t (e^{-n\Delta t/\tau} + e^{-(n-1)\Delta t/\tau} + \dots + e^{-\Delta t/\tau}), \quad (14)$$

which is a geometrical progression, the sum of which can be written in closed form:

$$(q^{n\Delta t} - q_s) = (q^0 - q_s) e^{-n\Delta t/\tau} + \alpha \Delta t \left[\frac{e^{-(n+1)\Delta t/\tau} - e^{-\Delta t/\tau}}{e^{-\Delta t/\tau} - 1} \right]. \quad (15)$$

The first term on the right-hand side of (15) is just any initial supersaturation reduced over n time steps by the parametrization. The second term is the combination of the dynamics source every time step being reduced by the parametrization in that and all subsequent time steps.

Assume that the initial state is saturated, $q^0 = q_s$, then (15) is just

$$(q^{n\Delta t} - q_s) = \alpha \Delta t \left[\frac{e^{-(n+1)\Delta t/\tau} - e^{-\Delta t/\tau}}{e^{-\Delta t/\tau} - 1} \right]. \quad (16)$$

At a fixed forecast time $T = n\Delta t$, the limit as $\Delta t \rightarrow 0$ is

$$(q^T - q_s) \rightarrow \tau \alpha (1 - e^{-T/\tau}). \quad (17)$$

Figure 1 shows the solution q^T for the dynamics source rate $\alpha = 0.5 \text{ h}^{-1}$ and the parametrization time-scale $\tau = 1 \text{ h}$. The solution is shown at elapsed times T of 1, 2 and 4 h and the limit $T \rightarrow \infty$, for a variety of time steps Δt : 4 h, 2 h, 1 h, 30 min, 15 min, 7.5 min, 5 min and 2.5 min, along with the limit $\Delta t \rightarrow 0$.

First we note that all the solution states are supersaturated. At a fixed forecast time T the solution q^T increases with decreasing time step. For a fixed time step, the solution increases with increasing forecast time T , reaching a finite limit as $T \rightarrow \infty$. None of these solutions represents the atmospheric-like state we are modelling, which is saturated. Except for the longest time step, the solution is far from an atmospheric-like trajectory that would be saturated. This is a rather unusual and undesirable model behaviour, where the approximate solution diverges farther from an atmospheric-like state as $\Delta t \rightarrow 0$ rather than converging closer to one. Of course, this is the solution for the parametrization as formulated in (4). The problem is due to that formulation (specifically the choice of time-scale) and the discrete time step. It simply does not return the model state to saturation fast enough relative to the source term to follow an atmospheric-like trajectory unless the time step is significantly longer than the assumed parametrization time-scale.

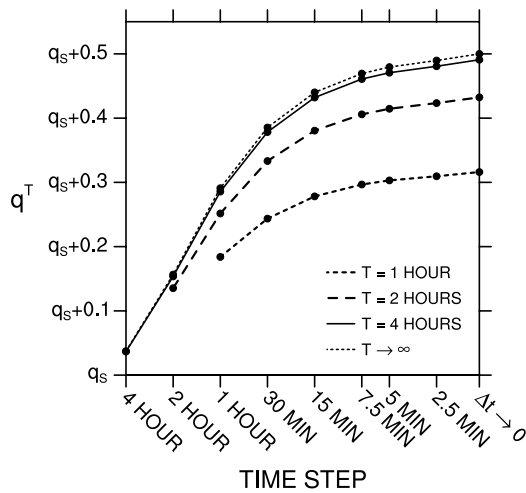


Figure 1. Solution of (16) with initial condition q_s at elapsed times T of 1, 2 and 4 h and the limit $T \rightarrow \infty$ as a function of time step Δt of 4 h, 2 h, 1 h, 30 min, 15 min, 10 min, 5 min and the limit as $\Delta t \rightarrow 0$.

We now consider a modification of this simple problem that makes it more like many AGCMs. We add an additional parametrization Q to (1):

$$\frac{dq}{dt} = D + P + Q, \tag{18}$$

where Q is a hard adjustment bringing the state to saturation if it is supersaturated, otherwise doing nothing:

$$q^{t+\Delta t} = \begin{cases} q_s & \text{if } q^t > q_s, \\ q^t & \text{if } q^t \leq q_s. \end{cases} \tag{19}$$

This additional term is more consistent with the continuous P described following (1). D and P are given as before by (3) and (5), respectively. We might think of P as a convection parametrization and Q as grid-scale condensation, as commonly included in AGCMs. The time-split sequence of approximations is then

$$q^* = q^{n\Delta t} + \alpha \Delta t, \tag{20}$$

$$(q^{**} - q_s) = (q^* - q_s) e^{-\Delta t/\tau}, \tag{21}$$

$$q^{(n+1)\Delta t} = q_s. \tag{22}$$

Again we assume $q^{n\Delta t}$ is at least saturated. Admittedly, given the form of Q (22), one may wonder why to bother with the parametrization P (21), but in a more complex model the parametrizations also affect other variables such as temperature and these are likely to be affected differently by P and Q , e.g. shallow or deep convection and prognostic cloud water in CAM4. The changes made by the split components are

$$\begin{aligned} q^* - q_s &= \alpha \Delta t, \\ q^{**} - q^* &= \alpha \Delta t (e^{-\Delta t/\tau} - 1), \end{aligned} \tag{23}$$

$$q^{(n+1)\Delta t} - q^{**} = -\alpha \Delta t e^{-\Delta t/\tau},$$

for D , P and Q , respectively.

Figure 2 plots these changes accumulated over a 4 h forecast for a variety of time steps. The parameters are the same as in the previous problem: $\alpha = 0.5 \text{ h}^{-1}$ and $\tau = 1 \text{ h}$.

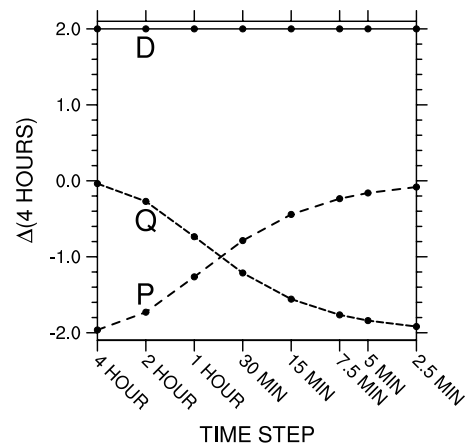


Figure 2. Changes made by the three components D , P and Q (23) over a 4 h forecast as a function of time step.

For a relatively long time step (4 h) compared to the time-scale of P (1 h), the parametrization P balances the dynamics source term and Q does very little, but for short time steps (5 and 2.5 min) the parametrization Q balances the dynamics source term and the parametrization P is effectively inactive. Of course with this simple problem it does not matter which parametrization removes the supersaturation. However, more complex parametrizations eliminate instabilities and supersaturation in different ways and affect other model variables such as temperature differently. If the state after the dynamics is such that P should be active, it is unreasonable for its effect to tend to 0 as $\Delta t \rightarrow 0$. It should remain active in removing the instability. As before, the problem is due to the formulation of the parametrization P . If the time step is relatively short, the assumed time-scale prevents the parametrization P from returning the model state to saturation in one application and the hard adjustment Q acts instead. We will see the consequences of this inconsistent behaviour in the CAM in the next section.

3. CAM simulations

We now describe and analyze the problem that was noticed in a high-resolution version of CAM4 and led to the considerations of the previous section. CAM4 (Neale *et al.*, 2011) with the spectral-transform dynamical core at $T340$ truncation and a time step Δt of 5 min experiences extreme truncation-scale cells of precipitation and upward motion in the Tropics, resembling ‘grid-point storms’ that have been alluded to in other models. However, these cells are not as long-lived in CAM4 as reported in other models and, although shorter lived, are perhaps more prevalent. At any one time there are usually several over the tropical oceans. Figures 3 and 4 show an arbitrarily chosen example of such an event. Figure 3 shows a time sequence of the vertical pressure velocity ω at 600 mb for a small region in the Tropics labelled with relative times 2.02–2.35 days. (Nominal time 0 days was a state taken from a long simulation and served as the initial condition for the simulations described here.) A truncation-scale, upward cell (negative ω) is seen forming after day 2 in the upper right corner and grows with time, reaching a strength of around $-1200 \text{ mb day}^{-1}$ at day 2.35. It moves westward and southward. The inner tick marks in the figures indicate the model transform grid points. Figure 4 shows the further development of this cell to day

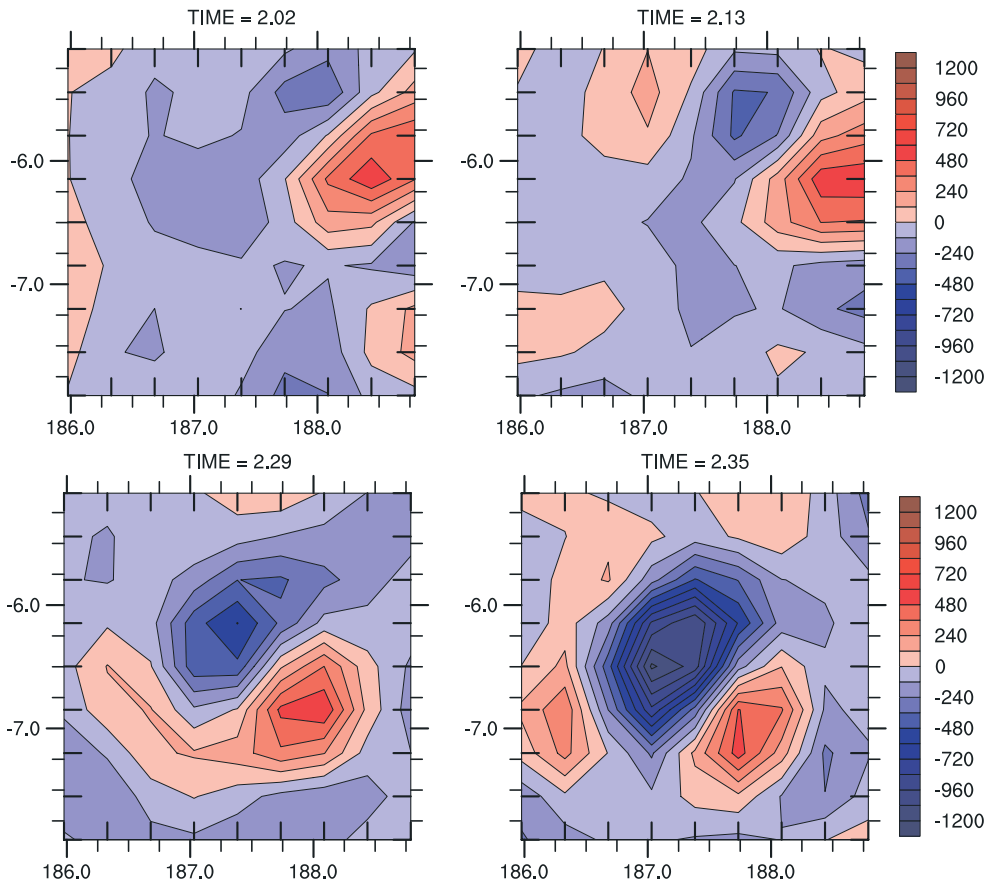


Figure 3. Pressure vertical velocity ω at 600 mb, contour interval 120 mb day^{-1} . Inner tick marks denote the transform grid points.

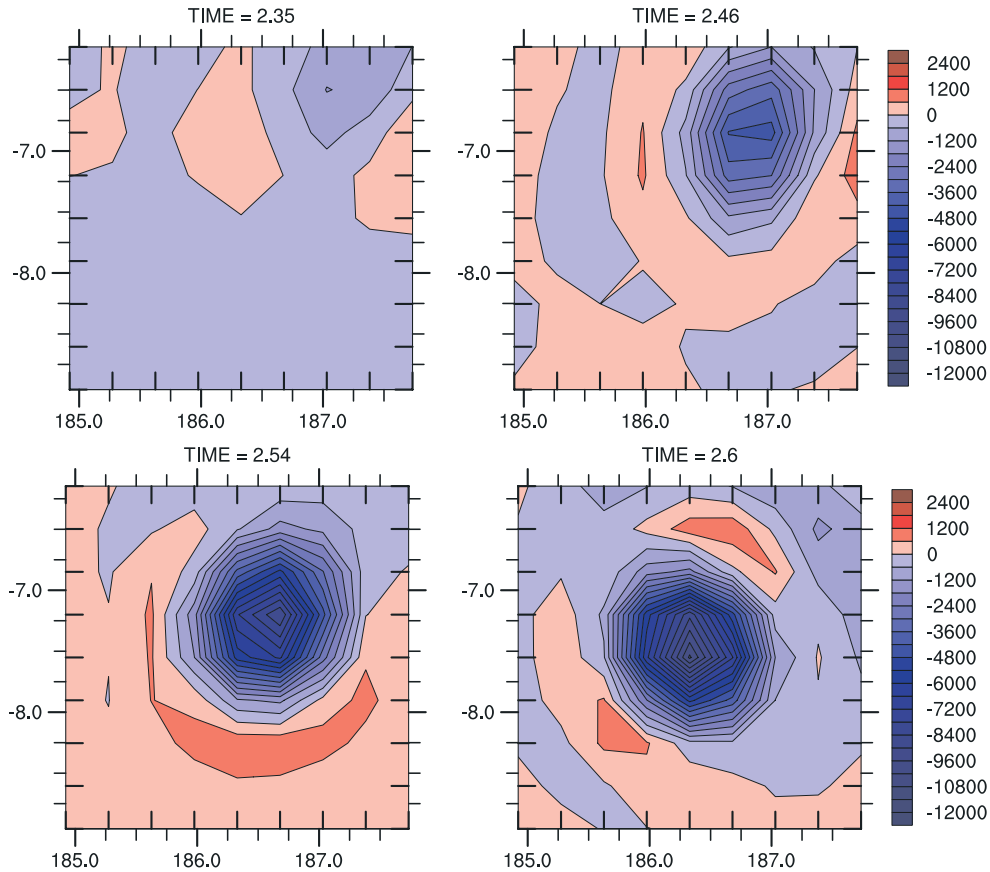


Figure 4. Pressure vertical velocity ω at 600 mb, contour interval 600 mb day^{-1} . Note: the upper left panel is the same field as in the lower right panel of Figure 3 but with a larger contour interval and shifted domain.

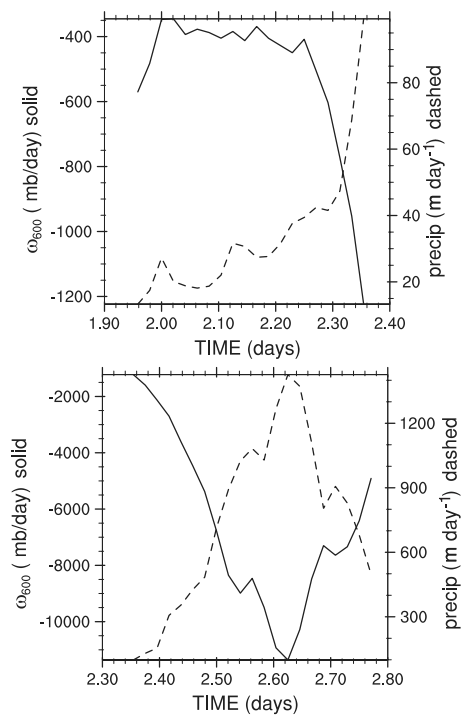


Figure 5. Pressure vertical velocity ω at 600 mb and precipitation in the centre of the moving cell.

2.6. Note that the domain and contour interval in Figure 4 differ from those in Figure 3. In fact, the field plotted in the upper left panel of Figure 4 is the same as that plotted in the lower right panel of Figure 3. In Figure 4 the cell continues to strengthen and move westward and southward. By day 2.6, ω in the centre of the cell reaches $-12\,000\text{ mb day}^{-1}$. We note that this is equivalent to $-42\text{ mb (5 minutes)}^{-1}$ and, since the vertical grid interval at 600 mb, computational instability is not an issue here. Relatively weak downward motion is seen surrounding the upward cell, which is indicative of gravity waves spawned by and propagating away from this explosively growing cell. These propagating waves are seen in animations of the simulation that originally attracted attention to this problem. After day 2.6 the cell starts to dissipate. This cell is typical of many seen in the simulation in the Tropics. Such cells are almost always popping up somewhere in the tropical domain.

Figure 5 shows the vertical velocity at 600 mb and the precipitation as a function of time following the centre of the cell. The centre at any time is defined to be the grid point with the strongest upward pressure vertical velocity, ω , at 600 mb. The top panel shows days 1.9–2.4 and the bottom shows days 2.3–2.8. Note that the ordinate is different in the two panels. Until day 2.25 the vertical velocity remains around -400 mb day^{-1} and the precipitation less than 35 mm day^{-1} but growing slightly. After day 2.3, both grow to extremely large values by day 2.6 with precipitation reaching 1400 mm day^{-1} and vertical velocity $-11\,500\text{ mb day}^{-1}$.

The CAM4 moist parametrization package consists of three processes applied sequentially. The first is the deep convection parametrization of Zhang and McFarlane (1995) modified by the addition of convective momentum transport by Richter and Rasch (2008) and by a dilute plume calculation by Neale *et al.* (2008). The second is the shallow

convection scheme of Hack (1994). We note that this parametrization can also serve as a deep convection scheme and was in fact used as such in CCM2 (Hack *et al.*, 1993). However, when applied after the Zhang and McFarlane scheme it is intended to deal with shallow and middle-level convection not treated by the deep convection. The third process is the prognostic cloud-water scheme developed by Rasch and Kristjánsson (1998) and Zhang *et al.* (2003). The deep and shallow convection parametrizations assume time-scales of 1 h and 30 min, respectively. The prognostic cloud-water scheme is designed to act more as a hard adjustment, especially when given a supersaturated state.

Figure 6 shows the vertical distributions of the moisture tendencies from these moist parametrization components as a function of time. Each convection tendency includes evaporation of rain created by that convection parametrization. The cloud-water tendency includes condensation and all other cloud-related processes such as conversion between cloud condensate and water vapour. The sampling is every 30 min and is at the grid column at the centre of the cell, following the cell. The tendencies are instantaneous values. The left column is from the deep convection, the middle from the shallow convection and the right from the prognostic cloud-water parametrization. This is also the order in which these components are called in the time-split parametrization suite. The top row shows the early period, days 1.95–2.11, before the cell grows explosively. The tendencies of the three processes are of similar magnitude, a few $\text{g kg}^{-1}\text{ day}^{-1}$, with seemingly reasonable vertical structures. They all behave differently from each other. The deep convection removes water from below 500 mb and at least part of the time deposits some above around 300 mb. The shallow convection moves vapour vertically locally, from the levels below 900 mb to that around 850 mb and from the level at 700 mb to that at 500 mb. (The inner tick marks in the figures indicate the location of the model levels.) The shallow convection parametrization also removes water vapour from the column. The cloud-water parametrization tendency is less vertically coherent, tending to remove vapour at single levels by creating condensate and stratiform rain and to add vapour at other levels by evaporating condensate and/or stratiform rain.

The pictures for all three tendencies are very different when the cell grows explosively between days 2.35–2.6, as can be seen in the bottom row of Figure 6. During this period, the three processes behave rather similarly, all condensing vapour to a large extent locally, i.e. with less vertical mixing, but with very different magnitudes. The prognostic cloud water reaches a maximum conversion rate of $-270\text{ g kg}^{-1}\text{ day}^{-1}$ at 600 mb while the shallow convection reaches a maximum of $-75\text{ g kg}^{-1}\text{ day}^{-1}$ at 600 and 700 mb. The deep convection has a similar shape but the maximum conversion rate occurs at higher levels around 400 mb with an even smaller maximum conversion rate of $-24\text{ g kg}^{-1}\text{ day}^{-1}$. During this period the corresponding temperature tendencies (not shown) are basically the mirror image, reflected about 0, of the moisture tendencies, indicating a release of latent heat dominating the small vertical mixing. Late in the period, the prognostic cloud-water tendency is due entirely to condensation creating rain. Conversions between cloud condensate and water vapour and changes in storage are negligible. The total moisture sink of these three processes is almost balanced by the

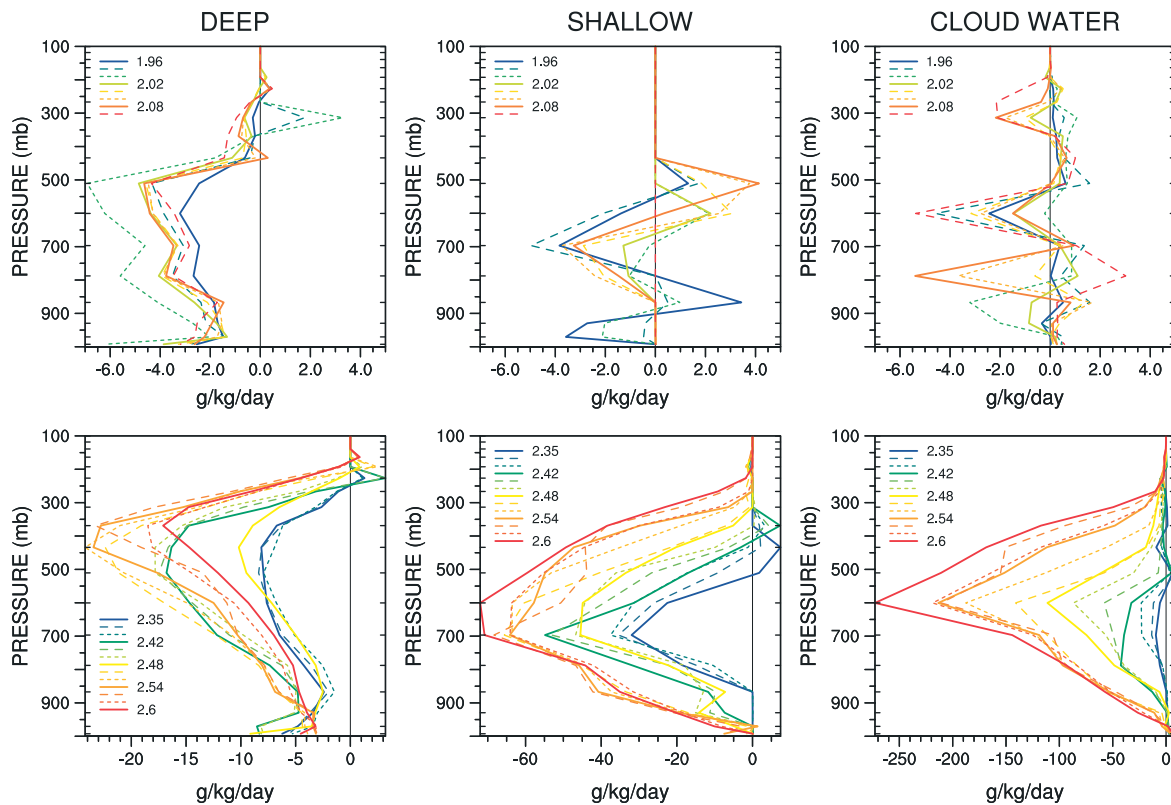


Figure 6. Moisture tendencies from deep convection, shallow convection and prognostic cloud-water parametrizations at the centre of the moving cell. Top row: days 1.96–2.11. Bottom row: days 2.35–2.6.

horizontal convergence and vertical advection of moisture by the dynamical component (not shown). The dynamical source is slightly larger at the beginning of the period, leading to a growth in precipitation. The parametrization sink becomes slightly larger when the cell dissipates after day 2.6. The release of latent heat drives the vertical motion seen in Figure 5. This is balanced by strong moisture convergence in the lower troposphere. This almost runaway situation requires both dynamics and parametrizations to occur. The dynamics cannot create such strong convergence without the heating from the parametrizations, and the parametrizations cannot create such strong heating without the moisture convergence from the dynamics. This coupling between vertical motion and release of latent heat seems related to the grid-scale convection problem reviewed by Manabe *et al.* (1965) to explain the need for convective adjustment in their early experiments. As they described it, grid-scale convection could not be resolved by the grid itself, so their computation quickly deteriorated. They added a convection scheme to break the direct link between vertical motion and condensation so that grid-scale convection did not develop. Of course, their grid was much coarser than is the case here. With the finer grid here, the model remains stable since the Courant–Friedrichs–Lewy (CFL) condition is not violated and it recovers from the strong vertical motion as the locally available water vapour is consumed. Direct calculation of convection requires a much finer grid. With enough resolution, such as cloud-resolving models, this dynamics–condensation interaction is the feedback required to produce resolved deep convection.

Now the relevance of the simple problems discussed in section 2 becomes obvious. From days 2.48–2.6, all three processes are trying to eliminate supersaturation. However,

the deep convection has a time-scale of 1 h and the shallow convection one of 30 min. The parametrization time step is 5 min. Thus, as seen in the simple problem, the deep and shallow convection remove very little of the supersaturation. The shallow convection removes more than the deep, in part because its time-scale is shorter, but both time-scales are relatively long compared to the time step. The cloud water makes a hard adjustment for supersaturated points and thus brings the state back to saturation. This is seen in Figure 7, which shows the evolution of the relative humidity in the grid column at the centre of the cell through the sequence of parametrizations. The first panel shows the relative humidity after the dynamics, before the moist parametrizations. The relative humidity becomes as large as 150% at day 2.6. The next panel shows the relative humidity after the deep convection, which has reduced it only slightly. The third shows the relative humidity after the shallow convection, which has reduced it to around 135% on day 2.6. Finally, the fourth panel shows the relative humidity after the prognostic cloud-water parametrization, which has brought it back to 100% each time step. Once again the two convection parametrizations are throttled by their imposed time-scales.

Of course, the convection parametrizations are designed to remove instabilities, not simply supersaturation. The shallow convection scheme (Hack, 1994) is based on a bulk, three-level, stability-dependent, non-entraining cloud model. When the bottom two levels are moist adiabatically unstable, it produces an adjustment to a stable stratification. The non-entraining convective element is rooted in the lower level, condensation and rain occur in the middle level and detrainment occurs in the top level. The three-level model is applied sequentially from bottom to top of the column, starting with the bottom three levels and shifting

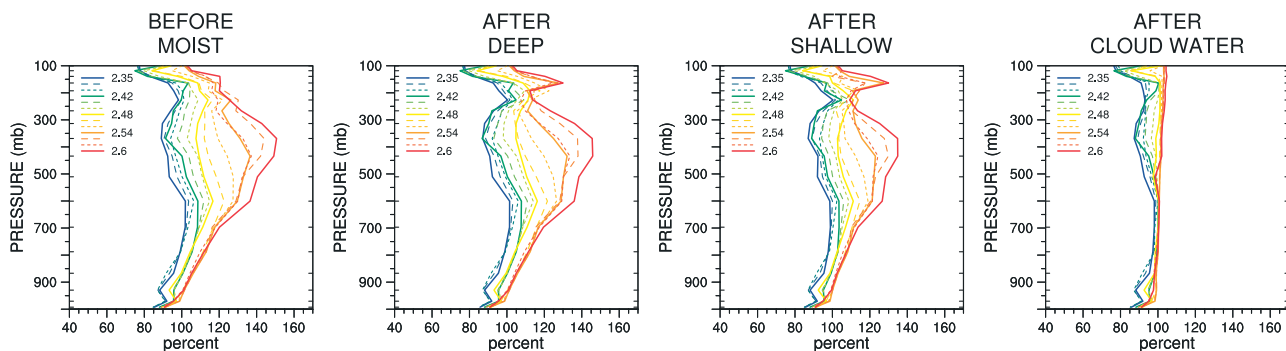


Figure 7. Relative humidity before the moist parametrizations, after the deep convection, after the shallow convection and after the cloud-water parametrizations at the centre of the moving cell.

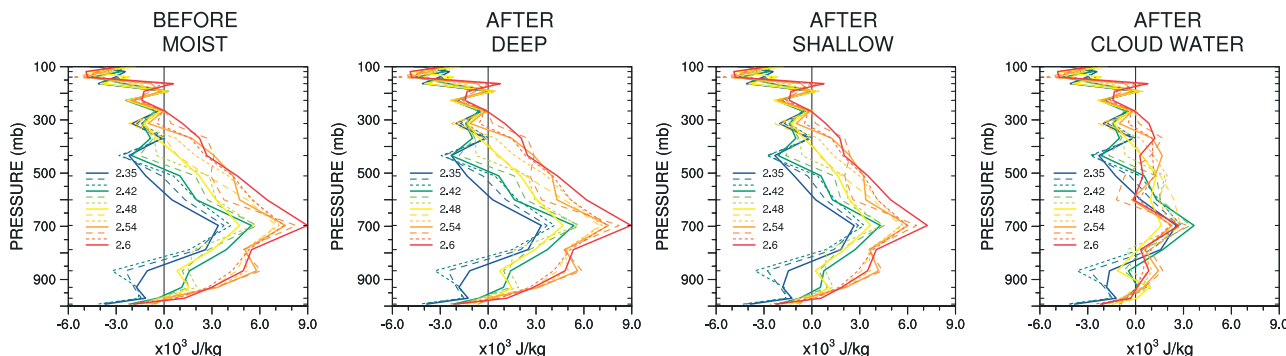


Figure 8. Stability measure $[h(k + 1) - h_s(k)]$ before the moist parametrizations, after the deep convection, after the shallow convection and after the cloud-water parametrizations at the centre of the moving cell.

up one level at a time. The shallow convection is active if the moist static energy at a level exceeds the saturated moist static energy at the level above (Hack, 1994). The moist static energy, h , is

$$h = C_p T + gz + Lq, \tag{24}$$

where T is temperature, z is geopotential height, q is specific humidity, g is the acceleration due to gravity, C_p is the specific heat capacity of dry air and L is the latent heat of vaporization. The saturated moist static energy, h_s , is

$$h_s = C_p T + gz + Lq_s, \tag{25}$$

where q_s is the saturated specific humidity. The shallow convection is active when

$$h(k + 1) + pert > h_s(k), \tag{26}$$

where k is the vertical grid index increasing downward and $pert$ denotes a perturbation that is added only when the convection is rooted in the boundary layer.

Figure 8 shows the evolution of $[h(k + 1) - h_s(k)]$ in the column at the centre of the cell sampled after each parametrization. We refer to this difference as the stability measure, positive implying unstable. The first panel of Figure 8 shows the stability measure after the dynamics, before the moist parametrizations. The measure is positive below 500 mb after day 2.5. By day 2.6, when the vertical velocity reaches its maximum, the stability measure is positive throughout the troposphere. This measure is barely affected by the deep convection, as seen in the second panel, but then this deep convection scheme is not necessarily designed to remove this type of instability.

The third panel shows the stability measure after the shallow convection. The shallow convection does reduce the measure at each time sample, but only by about 20%. The shallow, however, is designed to release the implied instability and to eliminate this difference but it assumes a 30 min time-scale. Finally, the fourth panel shows the stability measure after the prognostic cloud-water parametrization. The cloud-water parametrization reduces the stability measure and the implied instability substantially, especially after day 2.5, even though such reduction is not intended as its principle function. Here again the shallow convection is not permitted to remove the instability completely because the assumed time-scale in its formulation is significantly larger than the time step. The cloud-water parametrization removes supersaturation locally, which significantly reduces $q(k + 1)$ from supersaturation to saturation and therefore reduces $h(k + 1)$ in (26), removing much of the instability but not all and leaving it much as it was before the moist processes earlier in the period.

A similar examination of CAPE (not shown) shows a significant amount of CAPE after the dynamics and before the moist parametrization suite, which is not eliminated by the deep convection. Again the assumed 1 h time-scale prevents the deep convection from significantly reducing the CAPE in the 5 min time step. Neither the shallow convection nor the prognostic cloud-water parametrization reduces the CAPE significantly. If anything, they tend to increase it and the following dynamics step tends to reduce it slightly, late in the period.

As an aside, we note that convection schemes not only affect moisture and temperature but also transport vertically, both upward and downward, cloud liquid and ice condensate, aerosols and chemical constituents. Thus

any constraint on the convection that is subsequently compensated for by the cloud-water parametrization may have a profound affect on other aspects of simulations.

We speculate that these truncation-scale extreme structures arise from a local condensational heating rather than from a vertical redistribution by convection, not all of which leads to condensation. In the simulation, when the cell grows strong enough and the state is highly supersaturated even the deep convection acts anomalously to be dominated by condensation, although its contribution to the total tendency is relatively small. We quantify this by calculating the vertical correlation of the temperature and moisture tendencies ($\partial T/\partial t$ and $\partial q/\partial t$) between 1000 and 100 mb. With only a release of latent heat, the two tendencies will be anticorrelated with a value -1 . The decrease in q from condensation is a scaled mirror image of the increase in T from the release of latent heat. If vertical mixing dominates, the correlation will be positive since both specific humidity and temperature decrease with height, but the correlation will not necessarily be $+1$ since the vertical gradients differ.

The top panel of Figure 9 shows the vertical correlation of the tendencies from the three parametrization components at the grid column following the centre of the cell. The anticorrelation of the deep convection tendencies (blue line) increases from -0.2 to -0.6 , being above -0.5 when the cell is around its maximum strength (day 2.4–2.6). This is also the period when the cell is supersaturated following the dynamics, before any parametrizations are applied (Figure 7). The bottom panel of Figure 9 shows the climatological frequency distributions of the vertical correlations of the three components over 150° – 225° longitude and -15° to $+15^\circ$ latitude for 6 days of three-hourly samples.

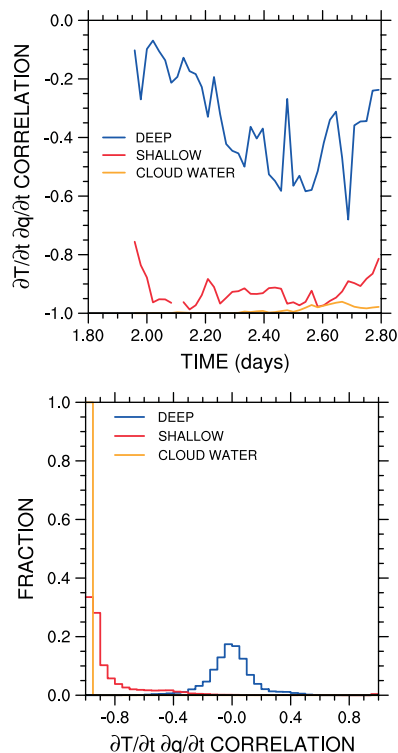


Figure 9. Top: Vertical correlation at the centre of the moving cell of the temperature tendency and moisture tendency for each parametrization. Bottom: Frequency distribution in bins of 0.05 of the vertical correlation of the temperature tendency and moisture tendency for each parametrization over 150° – 225° longitude and -15° to 15° latitude for 6 days of three-hourly samples.

Note that this region and period include strong cells such as the one examined here, but those cells do not dominate the distributions. The deep convection climatological frequency distribution is centred around 0 with a slightly negative peak and becomes very small for correlations >0.35 in magnitude. When the cell is growing (after day 2.20), the anticorrelation at the centre of the cell (top panel) is greater than -0.35 . Thus the values at the centre of the cell represent rare events, indicating that the deep convection is behaving in an unusual manner with more condensation than is typical. It is also unclear whether the convection is designed to work well in a strongly supersaturated environment such as that seen in the cell centre.

The anticorrelation of the tendencies from the shallow convection at the centre of the cell is above -0.9 except at the beginning and the end of the period (top panel, Figure 9, red line). It is not -1 because, as described above, in the three-layer conceptual model the parametrization includes moisture detrainment into the third layer, which does not affect temperature. In addition mixing occurs between the first and second layers. The condensation occurs in the second or middle layer. The climatological anticorrelation of the shallow convection is above -0.9 more than half of the time, so the shallow parametrization in the cell centre column is perhaps a little uncommon, but not necessarily extreme.

The cloud-water anticorrelation at the centre of the cell is above -0.95 for the entire period (yellow line). Often it is nearly -1 . It is not identically -1 , since the parametrization includes some processes that involve T but do not involve q such as transformations between cloud liquid and cloud ice. The climatological anticorrelation of the cloud water is always above -0.95 for the tropical region considered here. (Note that the bin size is 0.05.) Thus these characteristics of the cloud-water parametrization are not unusual even though its strength is.

4. Sensitivity studies

Because of the long time-scales compared with the time step, neither convection parametrization removes the moist instabilities via vertical redistribution and condensation. Thus the prognostic cloud water removes all supersaturation, yielding local condensational heating with no vertical redistribution. This strong heating on scales near the truncation limit drives strong vertical motion with accompanying strong moisture convergence. This leads to a vicious circle at these scales between the dynamics source and the parametrization sink, each becoming stronger from days 2.35–2.6. We hypothesize that this strong feedback between the condensational heating and dynamical convergence might not occur if the convective parametrizations were allowed to release the instabilities fully and return the model state to an atmospheric state by the end of each time step.

To test this hypothesis, we ran a simulation in which, beginning on day 2, we set the time-scales of both convection parametrizations equal to the time step. While this should make the convection parametrizations more active, Figure 2 shows that for the parametrization with the time-scale (P) to dominate the adjustment parametrization (Q) the time-scale needs to be one half to one quarter of the time step. Thus we do not expect to see the full effect here. Nevertheless, this should provide an indication of whether the problem is less severe with shorter time-scales. After a rather violent adjustment as the model transitions

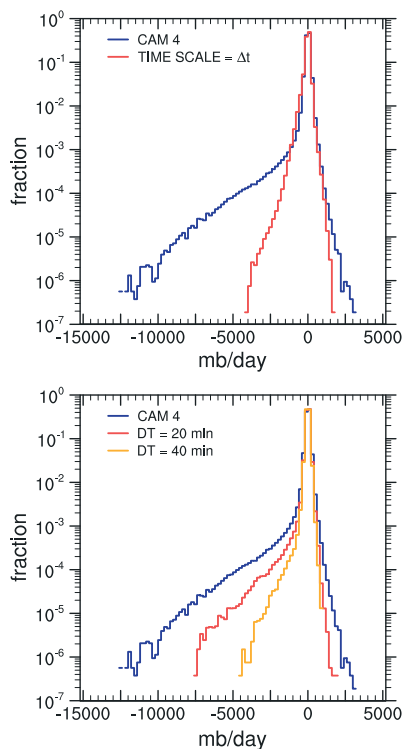


Figure 10. Frequency distribution of pressure vertical velocity ω at 600 mb over 150° – 225° longitude and -15° to 15° latitude for 6 days of three-hourly samples.

to states consistent with these modified parametrizations, no strong cells were observed. To quantify this subjective observation, the top panel in Figure 10 shows the frequency distribution of the pressure vertical velocity at 600 mb from the original simulation (blue and labelled CAM4) and from the modified simulation (red and labelled TIME SCALE = ΔT). The distributions were calculated over the region 150° – 225° longitude and -15° to $+15^{\circ}$ latitude, and over 6 days of three-hourly samples after the simulations reached their own climate. The figure shows that the maximum upward vertical velocity at 600 mb in the original simulation is $-12\,500\text{ mb day}^{-1}$, even greater than in the particular example we studied above. The modified simulation has a maximum upward velocity of -4000 mb day^{-1} , three times smaller.

The top row of Figure 11 shows the frequency distribution of the total precipitation and its convective and large-scale components. The maximum total precipitation decreases from 1750 mm day^{-1} in CAM4 to 800 mm day^{-1} in the modified simulation, although there are very few samples above 600 mm day^{-1} . (A gap in the curve indicates no occurrence of that rate.) We think it is unreasonable for events as strong as 1750 mm day^{-1} to occur once or more in 10 days. The Tropical Rainfall Measuring Mission (TRMM) 3B42 data set (available from http://mirador.gsfc.nasa.gov/collections/TRMM_3B42_006.shtml), which is of comparable resolution in space and time, includes events this large, but they occur 100 times less frequently. In the control run (CAM4) the large-scale precipitation matches the total and the convection contributes very little. With the reduced time-scales, the maximum values of the large-scale precipitation decrease by around a factor of 4. The maximum value of the convective precipitation increases from around 150 mm day^{-1} to around 500 mm day^{-1} . Note

that the frequency distributions of the two precipitation components in the modified simulation are very similar, with the convective having slightly larger maximum values. The distribution between large-scale and convective precipitation has completely changed.

Changes in the partition between individual parametrization components have also been noted at lower resolutions in climatological average precipitation when the time-scale of one process is modified. Mishra and Srinivasan (2010) report a change in the partition between deep and shallow convective precipitation in the equatorial average in long climate simulations, when the time-scale of the deep convection is changed but the time-scale of the shallow is held fixed. Their experiments were with the semi-Lagrangian spectral transform version of CAM3 at $T63$ truncation with a 60 min time step. With the standard 1 h time-scale for the deep convection, it dominated and the shallow convective precipitation was near zero. As the time-scale increased above 2.5 h, the deep convection component decreased and the Hack ‘shallow’ increased so that with a six-hour deep convection time-scale the average precipitation produced by the two components was about equal. With longer deep convection time-scales the ‘shallow’ scheme began to dominate. The Hack shallow scheme is capable of approximating deep convection and in fact was the deep convection scheme in CCM2 (Hack *et al.*, 1993). Again, as the time-scale increases the deep convection parametrization becomes more constrained and less active.

Another way to reduce the discrepancy between the time-scale and the time step is to increase the time step while keeping the time-scales at the values of the standard model. Previously, in the Eulerian spectral transform version of CAM, the dynamics and parametrization had to have the same time step. The 5 min time step was chosen to maintain computational stability of the dynamical core. Recently, the model was modified to allow the dynamics to substep the parametrizations. Thus we can now run the parametrizations with 20 and 40 min time steps while keeping the dynamics time step at 5 min to maintain stability. The bottom panel in Figure 10 and the bottom row of Figure 11 show the frequency distributions of vertical velocity and precipitation, respectively, from simulations with 5, 20 and 40 min time steps, all with the original CAM4 convection parametrizations time-scales. As Δt increases from 5 to 20 to 40 min, the maximum vertical velocity at 600 mb decreases as hypothesized. Similarly the maximum total precipitation and large-scale precipitation decrease. The convective precipitation shows little variation with time step. This implies the convection is releasing the instability by vertical mixing, rather than just by release of latent heat.

Climate simulations with CAM at coarser resolution have also shown sensitivity to the time step, with a decrease in the space–time average of convective precipitation with decreasing time step. At the same time, the stable precipitation increases even more to yield an increase in total precipitation with decreasing time step. Williamson (2008) observed this redistribution in the global average precipitation in standard Eulerian spectral transform CAM3 aqua-planet experiments at a variety of horizontal resolutions. Mishra and Sahany (2011) observed a similar behaviour in the tropical average precipitation with the semi-Lagrangian spectral transform version of CAM3 in Earth-like simulations at $T63$ truncation. This behaviour is consistent with the convection becoming less active and thus

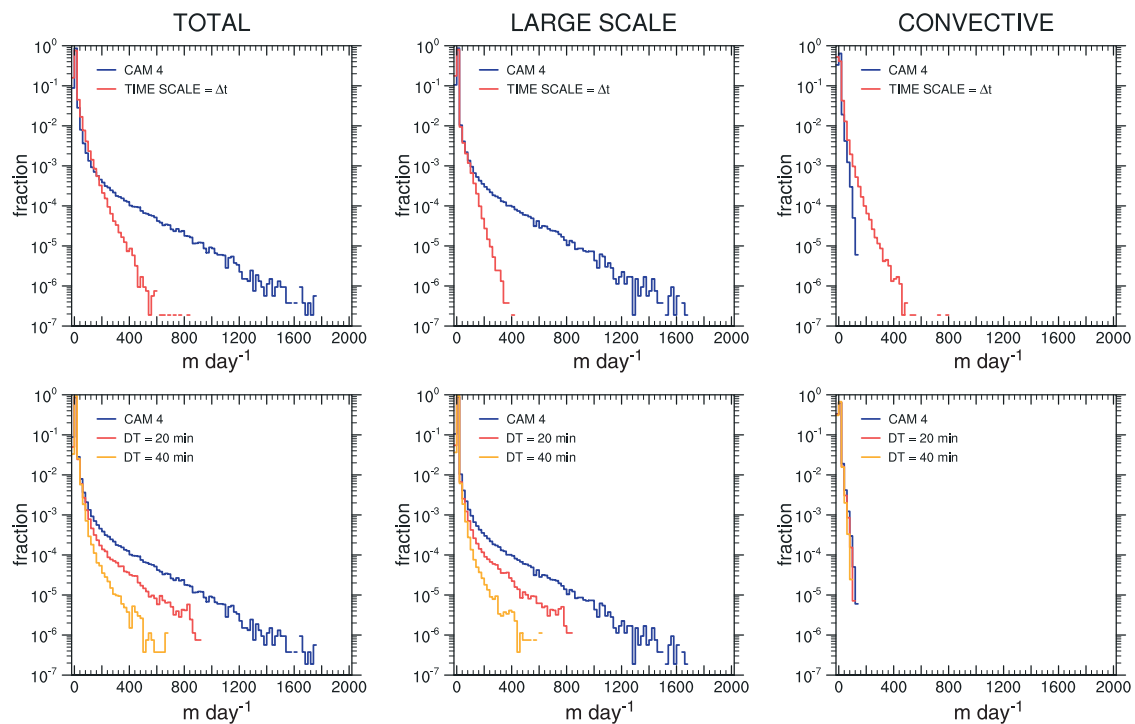


Figure 11. Frequency distribution of total, large-scale and convective precipitation over 150° – 225° longitude and -15° to 15° latitude for 6 days of three-hourly samples.

performing less vertical redistribution and condensation of water vapour with the shorter time steps, while the stable precipitation becomes more active to compensate.

Although a sensitivity is seen in the average precipitation at lower resolutions, we do not see the strong dependence on time-scale of the extreme precipitation in the frequency distribution. We repeated the two simulations discussed at the beginning of this section in conjunction with the top panel of Figure 10 at $T85$ truncation instead of $T340$. Both used a 5 min time step. One simulation used the standard CAM4 1 h and 30 min time-scales for the deep and shallow convection parametrizations, respectively. The other simulation set both time-scales to 5 min. The two frequency distributions (not shown) of vertical motion at 600 mb were similar to each other, not indicating the strong sensitivity seen in the top panel of Figure 10 for $T340$. In fact, the distribution for the run with short time-scales had slightly larger values for the extreme vertical motion, but the values and difference were small compared with $T340$, being -1700 and -2000 m day^{-1} for the standard and short time-scales, respectively. This structure was mirrored in the total precipitation and both components. We speculate that this different behaviour is because the coarser resolution cannot support the strong horizontal convergence near its truncation limit that developed in the $T340$ simulations and thus the strong interaction between the dynamics and parametrizations does not set up.

5. Conclusions and discussion

We have examined a problem akin to grid-point storms that occurs in high-resolution ($T340$) simulations with CAM4 when run with a relatively short time step. The problem manifested itself as extreme truncation-scale vertical motion and precipitation that spawned outward-propagating gravity waves most noticeable in animations. The problem was

traced to the fact that individual parametrizations did not work to return the state to an atmospheric-like trajectory. They were restrained by the time-scales assumed in their formulations, which were appreciably longer than the model time step. The deep and shallow convection parametrizations are applied with time-scales of 1 h and 30 min, respectively. The $T340$ spectral transform model time step was 5 min. Since the convection parametrizations did not remove the instabilities and supersaturation, the prognostic cloud-water scheme, which is not constrained by a time-scale, did remove supersaturation. The associated local release of latent heat drove very strong vertical motion and horizontal convergence, which transported even more water vapour into the column.

Two simple model problems were introduced that illustrate the ramifications of the mismatch of the time-scale and time step. The first simple model predicts specific humidity q with two processes that we refer to as dynamics and parametrization. We envision the continuous problem as being steady-state with saturated specific humidity q_s resulting from the dynamics providing a source that is balanced by a parametrized sink (condensation). In this problem the dynamics provides a linear increase of q with time and can be considered exact. The parametrization, however, is approximated by assuming it removes supersaturation with a specified time-scale. The two components are coupled in a time-split manner. In each time step the parametrization does not return the state to saturation unless the time step is very long compared with the time-scale. At a fixed time, as the time step decreases the supersaturation increases. This occurs because, for example, if the time step is divided in half then the dynamics produces the same increase divided over two smaller steps, but because of the assumed time-scale the parametrization removes less than half in each of the two smaller steps. The smaller the time step, the larger the supersaturation at a fixed

forecast time. Normally, in discrete modelling, we expect the solution to converge to an atmospheric-like state as the time step approaches zero, but here it diverges.

The other model problem adds a second parametrization to the first simple model. This second parametrization is applied after the first and is a hard adjustment bringing a supersaturated state back to saturation. The net result is always to end with a saturated state, but the partition between the two parametrizations is very different depending on the time step. If the time step is very long compared with the time-scale of the first parametrization, the first parametrization does all the work and the second does very little. If the time step is short compared with the parametrization time-scale then the second does all the work and the first does very little. In the simple model the final state is the same, but in an atmospheric AGCM the two parametrizations do much more than simply remove supersaturation. For example the convection parametrizations, which in CAM4 involve specified time-scales, eliminate instabilities and provide vertical mixing of cloud water, aerosols and chemical constituents while the prognostic cloud scheme in CAM4 operates more as a local hard adjustment when supersaturation is present.

We examined the behaviour of the moist parametrization components in CAM4 in detail for one strong cell. When the cell was growing to its maximum intensity, the specific humidity tendencies from the deep convection, shallow convection and prognostic cloud water parametrizations all had similar structures but the strengths were very different. Their maximum intensities were -24 , -75 and $-279 \text{ g kg}^{-1} \text{ day}^{-1}$, respectively. Examination of the relative humidity before each process shows that the value after the dynamics and before the parametrizations were applied was around 150%. The deep convection reduced it slightly, after which the shallow reduced it to around 135%. Both of these components were constrained from performing vertical mixing and eliminating the supersaturation by their time-scales. Finally, the prognostic cloud water eliminated the supersaturation. We further examined the stability measure that drives the shallow convection and showed that it is reduced only slightly by the shallow convection, rather than being eliminated. Again, because the time-scales limited the convection, the prognostic cloud water has a much larger effect on the stability measure by eliminating the supersaturation.

We argue that due to the long time-scales compared with the time step, neither convection parametrization removes the moist instabilities via vertical redistribution and condensation. The prognostic cloud water removes all supersaturation, yielding local condensational heating with no vertical redistribution. This strong heating drives strong vertical motion with accompanying strong moisture convergence. In models such as CAM4 at truncations unable to resolve deep convection properly, this leads to a vicious cycle in which both the dynamics source and the parametrization sink become stronger. We hypothesize that this strong feedback between condensational heating and dynamical convergence might not occur if the convective parametrizations were allowed to release the instabilities fully and return the model state to an atmospheric state at the model resolved scales by the end of each time step. This hypothesis was supported by a second simulation in which the convection time-scales were set equal to the time step. In this simulation, the maximum vertical velocity was

reduced by a factor of three and no excessive cells were observed. The same effect was seen when the time step was increased from 5 min to 40 min while keeping the original convection time-scales unchanged. Thus we believe the fast moist process parametrizations should be formulated to remove instabilities and supersaturation in a single time step, i.e. in a given time step the parametrizations should remove any instabilities or supersaturation introduced in that time step by the dynamics or other parametrizations such as radiation or surface fluxes.

There is no reason to expect this problem to be less serious when the parametrization components are process-split. In process-split approximations, each component is given the same state to work from rather than the state created by the previous component. In the model situation examined in section 3 the process-split combination might result in more condensation than produced by the time-split combination. This is because each component will not reduce the supersaturation before the next process is applied and the subsequent processes therefore make larger changes. Thus, when the process-split tendencies are combined, the total parametrized condensational heating will be greater than with time-splitting and drive even stronger vertical motion and moisture convergence. On the other hand, when the combined moisture tendency is subtracted from the initial state, the updated state will be subsaturated rather than just saturated. The following dynamics step will be starting from a subsaturated state rather than a saturated one and that difference may be enough to offset the extra moisture convergence.

Zhang and McFarlane (1995) chose 2 h for the adjustment time in their parametrization for their model using a 20 min time step based on a few monthly simulations. Their criterion was 'that the precipitation regime in the tropics is predominantly convective while preventing excessive stabilization due to the choice of a value which is too small'. However, their calibration experiments were at a very coarse horizontal resolution of $T32$ spectral truncation, as reported for their control (McFarlane *et al.*, 1992). This configuration is even coarser than our $T85$ described above, which did not show the strong truncation-scale feedback between the dynamics source and parametrization heating. We do not argue that the Zhang and McFarlane (1995) scheme itself should necessarily adopt a very fast time-scale. Perhaps that is inappropriate for the parametrization as it is formulated, e.g. a plume developing through the depth of the troposphere. Instead we argue that the convection parametrizations should be reformulated.

We believe that the moist process parametrizations should be formulated to keep the model on an atmospheric-like trajectory at the scales resolved by the model. Thus we believe that they should complete their action in one time step and respond to any instabilities or supersaturation that develop in a time step. Presumably, the shorter the time step, the smaller the tendencies of these processes will be. Whether current parametrizations are suitable for or capable of doing this in a consistent way is another issue.

The atmosphere itself evolves continuously, with the processes involved continually responding to and partially balancing each other. In modelling fluid flow, we expect the model to approach this continuous behaviour as the grid sizes tend to zero. Such convergence generally implies that the grids in all dimensions, space and time, tend to zero simultaneously. With good approximations one would

expect the solution to approach reality as the grid sizes tend to zero, with processes working as believed to and observed to work in the atmosphere. It is not clear how to take this limit spatially with AGCMs, which include an unresolved parametrized component. However, we would hope that, when the spatial resolution is held fixed, as the time step alone goes to zero the solution would approach a reasonable semi-discrete approximation to the atmosphere and the partition between moist processes would be reasonable and as expected for the spatial scales included. If all the moist parametrization components assume fixed time-scales then the solution will often not be like the atmosphere at the modelled spatial scales, unless the time step is long compared with the time-scales. If some components assume a fixed time-scale but at least one is formulated to complete its action in one time step, as in CAM4, then the partition between components will be unreasonable in the limit as the time step approaches zero. An unreasonable partition could have profound effects on other aspects of the simulation. For example, if the convection becomes small its contribution to the vertical transport of cloud liquid and ice condensate, aerosols and chemical constituents would become small as well.

A decrease in convective transport is unlikely to be compensated for by the resolved vertical advection with the spatial resolution considered here. The upward component might be compensated for partially, but the vertical distribution is likely to be different. Downward transport would be very different. The plot of vertical velocity at 600 mb (Figure 4) shows very little downward motion at the grid points near the upward cell. Presumably the downward motion compensating for the upward cell is large-scale and remote through the Hadley and Walker circulations. The convection parametrizations, on the other hand, provide local downward constituent transport through subsidence in the environment around the updraughts to produce zero net mass flux through the layer in the grid cell and transport by convective downdraughts with corresponding compensating ascent in the environment. Therefore the vertical transport of cloud condensate, aerosols and chemical constituents will be very different depending on whether parametrized convection occurs in models with these resolutions.

Acknowledgements

I thank Richard Neale and Philip Rasch for discussion on the parametrizations in the CAM and Terry Davies for discussions on grid-point storms. I also thank John Truesdale and Julie Caron for pointing out the truncation-scale storms in the T340 CAM4 and John Truesdale for running the experiments. Christiane Jablonowski, Mark Taylor, Warren Washington, Peter Caldwell, Brian Medeiros and two anonymous reviewers provided helpful comments that led to improvements in the original manuscript. This research was partially supported by the Office of Science (BER), US Department of Energy, Cooperative Agreement No. DE-FC02-97ER62402. This research used resources of the Oak Ridge Leadership Computing Facility, located in the National Center for Computational Sciences at Oak Ridge National Laboratory, which is supported by the Office of Science (BER) of the Department of Energy under Contract DE-AC05-00OR22725.

References

- Collins WD, Hack JJ, Boville BA, Rasch PJ, Williamson DL, Kiehl JT, Briegleb B, McCaa JR, Bitz C, Lin S-J, Rood RB, Zhang M, Dai Y. 2003. 'Description of the NCAR Community Atmosphere Model (CAM2)'. National Center for Atmospheric Research: Boulder, CO. Available from: <http://www.cesm.ucar.edu/models/atm-cam/docs/cam2.0>
- Collins WD, Rasch PJ, Boville BA, Hack JJ, McCaa JR, Williamson DL, Kiehl JT, Briegleb BP, Bitz CM, Lin S-J, Zhang M, Dai Y. 2004. 'Description of the NCAR Community Atmosphere Model (CAM3.0)', Tech. Rep. NCAR/TN-464+STR. National Center for Atmospheric Research: Boulder, CO. Available from <http://www.cesm.ucar.edu/models/atm-cam/>
- Collins WD, Rasch PJ, Boville BA, Hack JJ, McCaa JR, Williamson DL, Briegleb BP, Bitz CM, Lin S-J, Zhang M. 2006. The formulation and atmospheric simulation of the Community Atmosphere Model Version 3 (CAM3). *J. Climate* **19**: 2144–2161.
- Hack JJ. 1994. Parameterization of moist convection in the National Center for Atmospheric Research Community Climate Model (CCM2). *J. Geophys. Res.* **99**: 5551–5568.
- Hack JJ, Boville BA, Briegleb BP, Kiehl JT, Rasch PJ, Williamson DL. 1993. 'Description of the NCAR Community Climate Model (CCM2)', Tech. Rep. NCAR/TN-382+STR. National Center for Atmospheric Research: Boulder, CO. Available from <http://library.ucar.edu/collections/technotes/>
- Kiehl JT, Hack JJ, Bonan GB, Boville BA, Briegleb BP, Williamson DL, Rasch PJ. 1996. 'Description of the NCAR Community Climate Model (CCM3)', Tech. Rep. NCAR/TN-420+STR. National Center for Atmospheric Research: Boulder, CO. Available from <http://library.ucar.edu/collections/technotes/>
- Kiehl JT, Hack JJ, Bonan GB, Boville BA, Briegleb BP, Williamson DL, Rasch PJ. 1998. The National Center for Atmospheric Research Community Climate Model: CCM3. *J. Climate* **11**: 1131–1149.
- Manabe S, Smagorinsky J, Strickler RF. 1965. Simulated climatology of a general circulation model with a hydrologic cycle. *Mon. Weather Rev.* **93**: 769–798.
- McFarlane NA, Boer GJ, Blanchet J-P, Lazare M. 1992. The Canadian Climate Centre second-generation general circulation model and its equilibrium climate. *J. Climate* **5**: 1013–1044.
- Mishra SK, Sahany S. 2011. Effects of time step size on the simulation of tropical climate in NCAR-CAM3. *Climate Dyn.* **37**: 689–704.
- Mishra S, Srinivasan J. 2010. Sensitivity of the simulated precipitation to changes in convective relaxation time-scale. *Ann. Geophys.* **28**: 1827–1846.
- Neale RB, Richter JH, Jochum M. 2008. The impact of convection on ENSO: From a delayed oscillator to a series of events. *J. Climate* **21**: 5904–5924.
- Neale RB, Richter JH, Conley AJ, Park S, Lauritzen PH, Gettelman A, Williamson DL, Rasch PJ, Vavrus SJ, Taylor MA, Collins WD, Zhang M, Lin S-J. 2011. 'Description of the NCAR Community Atmosphere Model (CAM 4.0)', NCAR Technical Note NCAR/TN-485+STR. National Center for Atmospheric Research: Boulder, CO. Available from <http://www.cesm.ucar.edu/models/ccsm4.0/cam/>
- Rasch PJ, Kristjánsson JE. 1998. A comparison of the CCM3 model climate using diagnosed and predicted condensate parametrizations. *J. Climate* **11**: 1587–1614.
- Richter JH, Rasch PJ. 2008. Effects of convective momentum transport on the atmospheric circulation in the Community Atmosphere Model, Version 3. *J. Climate* **21**: 1487–1499.
- Sportisse B. 2000. An analysis of operator splitting techniques in the stiff case. *J. Comput. Phys.* **161**: 140–168.
- Strang G. 1968. On the construction and comparison of difference schemes. *SIAM J. Numer. Anal.* **5**: 506–517.
- Williamson DL. 2002. Time-split versus process-split coupling of parametrizations and dynamical core. *Mon. Weather Rev.* **130**: 2024–2041.
- Williamson DL. 2007. The evolution of dynamical cores for global atmospheric models. *J. Meteorol. Soc. Jpn* **85B**: 241–269.
- Williamson DL. 2008. Convergence of aqua-planet simulations with increasing resolution in the Community Atmosphere Model, Version 3. *Tellus* **60A**: 848–862.
- Zhang GJ, McFarlane NA. 1995. Sensitivity of climate simulations to the parametrization of cumulus convection in the Canadian Climate Centre general circulation model. *Atmos. – Ocean* **33**: 407–446.
- Zhang M, Lin W, Bretherton CB, Hack JJ, Rasch PJ. 2003. A modified formulation of fractional stratiform condensation rate in the NCAR Community Atmosphere Model (CAM2). *J. Geophys. Res.* **108**: 4035. DOI:10.1029/2002JD002523.